ISSN 1990-3413, Astrophysical Bulletin, 2011, Vol. 66, No. 1, pp. 109–122. © Pleiades Publishing, Ltd., 2011.
Original Russian Text © P.G. Tsybulev, 2011, published in Astrofizicheskij Byulleten, 2011, Vol. 66, No. 1, pp. 118–133.

# New-Generation Data Acquisition and Control System for Continuum Radio-Astronomic Observations with RATAN-600 Radio Telescope: Development, Observations, and Measurements

**P. G. Tsybulev***

*Special Astrophysical Observatory, Russian Academy of Sciences, Nizhnij Arkhyz, 369167 Russia*

Received June 10, 2010; in final form, August 9, 2010

**Abstract**—A new Data Acquisition and Control System for performing continuum radio-astronomical observations with the RATAN-600 radio telescope is presented. One of the "building blocks" of the system is the Embedded Radiometric Data Acquisition System (ER-DAS) developed at the RATAN-600. It is a measurement facility meant for digitizing and reducing radiometer signals and for transmitting the result of these operations via Ethernet networks. ER-DAS system is shown to have a low self-noise level and to lack $1/f$-type noise. The measurement facility is shown to operate efficiently in radio-astronomical observations. Radiometric measurements of the parameters of high-sensitivity radiometers are illustrated in the case of the measurements of radiometer gain fluctuations.

**DOI:** 10.1134/S199034131101010X

Key words: *techniques: radar astronomy—methods: data analysis*

## 1. INTRODUCTION

The Data Acquisition and Control System (DACS) for radio-astronomical observations at the RATAN-600 radio telescope is a complex hardware and software facility and ocuupying a large surface. The currently operating DACS for continuum observations was developed in early 1990s [1] and has undergone repeated upgrades since then. The emergence and introduction of new high-speed Digital Signal Processing (DSP) facilities has resulted in a qualitative breakthrough in this field. It became possible to actively intervene into the process of the normalization of the output signals of radiometers, e.g., in the case of impulse noise filtering [2–5]. The need for a new DACS is caused by a number of factors. The most important of these factors include:

- changes in the composition and architecture of continuum radiometer facilities of the RATAN-600, which impose new requirements to DAC;
- ageing and obsolescence of the existing hardware and software DACS;
- heterogeneous hardware and software used in different radiometric facilities;
- the need for extending the set of possible observational modes;
- increased radio interference in the vicinity of the radio telescope, which makes necessary the development of facilities and techniques for active protection of the operating bands of the RATAN-600.

The aim was to develop a DACS based on modern radio-technical hardware components and modern approaches to the deployment of distributed computing environment needed to adequately address the tasks of data acquisition and control both in radiometric facilities and in the process of observations with the radio telescope. Our other tasks were to improve the accuracy of the measurement of the radiometer signal, extend the available set of observational methods and preliminary data reduction, and achieve certain unification of the hardware and software used in DACS.

Below we show how these problems are addressed on the RATAN-600 and demonstrate the results of the application of the upgraded DACS in radiometric measurements and radio-astronomical observations.

## 2. EMBEDDED DATA ACQUISITION SYSTEM OF THE RADIOMETRIC FACILITY—ER-DAS

Several continuum radiometric facilities are available at the RATAN-600 radio telescope, and new

*E-mail: peter@sao.ru

ones are regularly added to the kit. Currently, there are three facilities in different receiving cabins ("feeds") at spatially separated locations, and all of them are located at a certain distance from the data collection center of the entire radio telescope. Each radiometric facility consists of several radiometric systems. Radiometric system consists of a single- or multichannel radiometer, a concrete engineering solution. At the stage of the planning of the new DACS the developers decided to equip every radiometric system with a standard unified device for the acquisition, control, and preliminary reduction of the data obtained in the process of radio-astronomical observations and radiometric measurements. Thus the notion of the DACS of a radiometric system was introduced.

The required DACS of the radiometric system was developed and manufactured in 2008–2009 and named the Embedded Radiometric Data Acquisition System (ER-DAS). To adequately describe the tasks addressed in this system, let us briefly discuss the technical aspects of the processing of the radiometric signal.

### *2.1. Processing of Radiometric Signal*

Currently, the continuum radiometers of the RATAN-600 are straight amplifiers of microwave signals within the given frequency band with square-law detection used to obtain the output signal proportional to the power of the received microwave radiation. Because of radiometer gain fluctuations various versions of circuits involving the modulation of the input microwave signal by a signal of the given form followed by synchronous demodulation at the output, like, e.g., in the classical radiometer of R. Dicke [6] shown in Fig.1a. Since a standard scheme of such signal reception is employed, the equipment set for processing the radiometer signal remains the same in terms of functionality. Its main components are:

- a Low-Frequency (LF) Preamplifier (video amplifier in Fig.1a);
- a Lock-In Detector in Fig.1a);
- a measuring device (currently, it is an analog-to-digital converter, ADC).

Note that in the switching radiometer the synchronous demodulation (extraction of the desired signal) is performed at the modulation frequency and at its harmonics, and therefore the LF preamplifier can be in the form of a video amplifier, transmitting the required spectral composition of the modulated signal, and cutting off the direct current (DC) component in the spectrum of the output signal of the square-law detector of the radiometer. The synchronous detector can be schematically represented as a multiplier of two signals (the radiometer signal and the modulation signal) followed by a Low-Pass Filter (LPF), as shown in Fig.1a (the unit named the Lock-In detector). Modulation is performed via the square wave signal with equal durations of the "high" and "low" levels with a period on the order of $1 - 10$ milliseconds. At the radiometer input this signal controls an electronic switch, whereas the lock-in detector performs synchronous multiplication of the modulated signal by $\pm 1$.

The Lock-In Detector (Lock-in) has long remained an analog signal-processing device, which had many weak points including:

- a precision analog Lock-in is difficult to make and setup; a professional analog Lock-in for research purposes is a complex and expensive instrument;
- the parameters of the Lock-in (like those of any analog device) drift with time;
- such a device is susceptible to ambient conditions (temperature, humidity, pressure);
- as we already pointed out above, the analog Lock-in operates without the DC component in the measured signal and therefore the information about the absolute value of the power of the radiation received by the radiometer during each particular modulation half-period is completely lost.

In 1995 a digital Lock-in detector was used for the first time at the RATAN-600 as a part of the equipment for the time-and-frequency interference mitigation in decimeter-wave radiometers [2, 4, 5] based on the noise-adding radiometer (NAR) scheme. To extract and remove the pulsed interference, the input signal had to be digitized at a high rate (on the order of several tens of kHz). Moreover, the output signal of the radiometer must contain a DC component, because interference in the NAR shows up only during the modulation half-period corresponding to the signal from the radio-telescope antenna (modulation half-periods become indistinguishable in the absence of a DC component in the signal). Therefore a DC preamplifier was introduced instead of the video amplifier in the analog signal path. Digitized signal is then processed by a high-speed digital signal processor (DSP), where synchronous detection of the signal is performed using the reference modulation signal.

The use of a DSP eliminated all the weak points of the analog Lock-in detector mentioned above: the

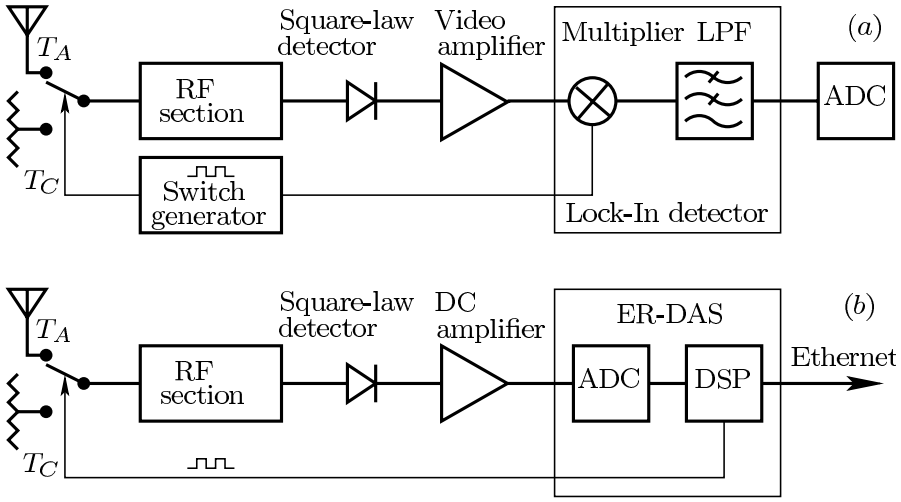


**Fig. 1.** (a)—Block diagram of the Dicke switched radiometer. Its components include the Square-Law Detector; LPF (Low-Pass Filter); ADC (Analog-to-Digital Converter); DAS (Data Acquisition System), and Lock-In detector (Lock-In). (b)—Modified scheme of the radiometer shown in panel (a): the output signal of the Square-Law Detector enters the DC amplifier and is then digitized in the ER-DAS (Embedded Radiometric DAS) system. Here DSP is the Digital Signal Processing unit.

parameters of the digital device and the software algorithms are immune to the interfering factors mentioned. Moreover, the modulation half-periods became distinguishable, thereby facilitating the diagnostics of radiometers and even making it possible to measure the equivalent noise temperature of the radiometer with a certain accuracy. However, the integrated DC amplifiers used at that time failed to ensure the sufficient measurement accuracy because of the zero drift due mostly to ambient temperature variations and the gain instability, which showed up as extra noise with a power spectral density (PSD) of the form $1/f^{\alpha}$, where $f$ is frequency.

### *2.2. Requirements to the New DACS of the Radiometric System*

The positive experience gained in the process of the operation of the Digital Lock-in Detector served as the basis for formulating the requirements to and the making of the new DACS of the radiometric system ER-DAS. The requirements to the new system are:

- the analog signal processing path should be based on precision DC amplifiers;
- the digitization of the signal before its digital lock-in demodulation should be performed at a sufficiently high speed to allow passing the sufficient number of harmonics of the modulation frequency and suppress, as far as possible, some kinds of interference, e.g., pulses;
- the analog signal processing path should contain a quality LPF to prevent frequency aliasing (anti-aliasing filter) in the process of the digitization of the radiometer signal;
- the Analog-to-Digital Converter must be located as close as possible to the radiometer output to prevent the effect of electromagnetic interference on the signal path;
- the ADC must be galvanically isolated from the Digital Lock-in Detector to prevent interference from the pulsed digital system from affecting the precision measurements;
- the DACS of the radiometric system must be embeddable into the radiometric system proper. Note that radiometers will perform the digitization and processing of signals autonomously;
- the DACS of the radiometric system should be network-ready and easy to integrate into the Local Area Network (LAN) to allow the transmission of digitized and reduced radiometer data and remote control of the radiometric system.

The practical realization of the above requirements leads us to the measurement and control system shown at the radiometer output in Fig. 1b. Here the "Video amplifier" is replaced by the "DC amplifier". Thus the information about the absolute signal power

at the radiometer output in each modulation half-period is fully preserved. The diagram in Fig. 1b shows the unit called ER-DAS (Embedded Radiometric Data Acquisition System). It includes the ADC unit and the DSP and communication (Ethernet) unit. The Lock-in demodulation of the radiometer signal in the Digital Lock-in detector is performed by a program of the digital signal processor.

### *2.3. Realization of the DACS of the Radiometric System—ER-DAS*

Figure 2 shows the block diagram of ER-DAS. The analog signal processing path, or, in other words, the signal conditioning path, consists of a precision DC amplifier followed by a fourth-order LPF with a Bessel characteristic and a 8 kHz cutoff frequency (such a characteristic is needed to transmit square-wave signals). The signal is then digitized in the 16-bit ADC at a rate of 32 thousand samples/s. The digitized signals of four analog channels are simultaneously transmitted via a galvanically isolated SPI (Serial Peripheral Interface) to the DSP processor. The DSP processor implements the algorithm of the lock-in detector followed by a substantial reduction of the sampling frequency (decimation) of the signal down to 128 samples/s from each channel. The data of four radiometric channels (or a smaller number of channels plus additional sensors) are transmitted to a dedicated back-end processor. The task of the front-end processor is to transmit the data via the Ethernet to the data acquisition center of the entire radiometric facility and to receive and execute external directives.

One of the tasks addressed in the system described consists in maximally accurate measurement if the DC component of the signal at the output of the square-law detector of the radiometer, because this measured quantity describes the total power of the microwave signal at the input of the square-law detector. This task cannot be successfully addressed without high-precision and inexpensive (given the large number of radiometric channels) DC amplifiers, because the signal should be amplified by a factor of $5 - 100$ prior to its measurement with the ADC. Special attention should be paid to the long-term stability of the parameters and the zero drift of the DC amplifier. The voltage to be measured at the output of the squared-law detector in the total-power radiometer is given by the following formula:

$$V = kBG\gamma\left[\frac{T_a}{L} + T_0(1 - \frac{1}{L}) + T_r\right] + V_0(t), \quad (1)$$

where $k$ is the Boltzmann constant; $B$, the microwave bandwidth of the radiometer; $G$, its total microwave gain; $\gamma$, the conversion factor of power to the voltage at the square-law detector; $T_a$, the noise temperature of the radiation at the radiometer input; $L$ ($L > 1$), the absolute losses in the input feed, which are equal to the input-to-output power ratio (for the feed); $T_r$, the noise temperature of the entire radiometer; $V_0(t)$, the stray voltage offset arising in the measurement system (after the square-law detector). Whereas the first term in (1) describes the total power of (external and intrinsic) radiation, the second term $V_0(t)$ introduces an absolute error, which, in addition, varies with time in the process of measurements performed using DC amplifiers. This is the so-called zero drift of the measuring system.

The system described here is the first such facility on the RATAN-600, where operational amplifiers (OpAmps) based on auto-zero technology—i.e., OpAmps with continuous zero calibration at a high frequency (on the order of 14 kHz) are use throughout the entire low-frequency path from the square-law detector to the ADC. These are precision OpAmps with very low intrinsic zero drift and extremely low thermal drift (three orders of magnitude lower than in best traditional OpAmps). Such an accuracy makes it possible to perform the zero calibration of the entire analog signal channel including the ADC and then measure only the true DC component of the output signal of the square-law detector.

Estimates of the achievable accuracy of the measurements of the DC component and a comparison with traditional OpAmps shows an improvement in the accuracy of more than two orders of magnitude. Thus a common OpAmp has an average thermal zero drift of about 0.6 $\mu$V/°C. Suppose that the constant component at the output of the square-law detector of a real uncooled radiometer with a system temperature of 470 K is equal to 5 mV. Thus the thermal zero drift of the radiometer expressed in Kelvins of the equivalent noise temperature in the case of a change of the physical temperature of the low-frequency path of the radiometer by $1°C$ is equal to $(0.6\ \mu\mathrm{V}/°C \times 470000\mathrm{mK})/5000\ \mu\mathrm{V} = 56.4\mathrm{mK}/°C$ (which is 20 times greater than the spectral density of the amplitude fluctuations of the best radiometer used at the RATAN-600). Here is the next example: the auto-zero OpAmp chosen for the system described here has an average thermal zero drift of $2\mathrm{nV}/°C$, which corresponds to $188\mu\mathrm{K}/°C$. This potentially means a 300 times better stability compared to the common OpAmp and is comparable to the sensitivity of the currently best available radiometers. Such an accuracy makes real the measurement of the absolute power of the radiation incident on the square-law detector, and, consequently, of the absolute temperature $T_s$ of the system in K provided accurate calibration of the radiometer and account of all sources of stray offsets of the DC component.

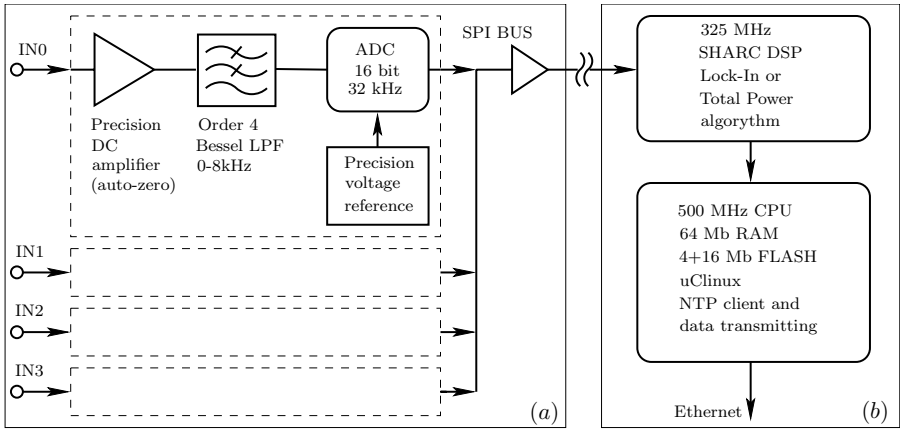


**Fig. 2.** The ER-DAS block diagram. The circuit consists of two galvanically isolated individual subsystems: (a)—the analog-digital subsystem; (b)—the DSP and communication subsystem.

Figure 3 illustrates the advantage resulting from the use of auto-zero OpAmps according to measurements made in practice. The ER-DAS system contains only auto-zero OpAmps in the analog signal channel and therefore the effect of connecting a traditional OpAmp becomes immediately apparent both in the signal and in the corresponding estimate of the spectral power density.

A certain rise of the spectral power density of the signal measured with auto-zero OpAmps at low frequencies (below 0.01 Hz) is not due to the measured amplifier, but to the DC source at the input of both amplifiers (see the measurement diagram in Fig.3a).

Thus the use of new electronic components allows the zero of the measurement system to be stabilized in time so that the absolute error of $V_0$ measurements in formula (1) becomes practically constant. As a result, the $V_0$ value can be measured and subtracted from the measured voltage (calibration of DC component in the measurement system).

Below we point out the following features of the realization of ER-DAS:

- in the signal normalization path with auto-zero OpAmp none of the active circuits introduce $1/f^{\alpha}$ type noise into the measured signal (see Figs. 3a and 3b) and therefore the main and only source of such noise in the real radiometer is the microwave path (microwave amplifiers and, possibly, the square-law detector). As a result, it is possible to measure real fluctuations $\delta G/G$ of radiometer gain ($G$);

- the entire measurement analog the path from the output of the square-law detector to the ADC (inclusive) is based on a circuit with unipolar (+5V) voltage. This choice was based on the fact that the signal of the half-wave square-law detector is fundamentally unipolar and the auto-zero amplifiers employed are based on rail-to-rail technology (they accurately measure the signal from one power rail to another) and have minimum possible intrinsic zero offset (2 $\mu$V);

- the signal conditioning path along with the ADC (Fig. 2) had the form of a measurement system (stable in time) that can be accurately calibrated in terms of the DC component of the signal, making it possible to achieve, in principle, the following correspondence: 0 Volts—0 degrees Kelvin, V Volts—T degrees Kelvin;

- the digitized data of the channels are transmitted to the DSP and communication subsystem along differential lines. The DSP subsystem can be located at a distance of up to 7 m from the radiometer output;

- the DSP processor that receives and processes the radiometer data operates in a single-task mode, which allows minimizing the response time for the events and incoming data;

- the communication processor operates under embedded uClinux OS [7], and is equipped with permanent memory for storing and loading the OS and the application software.

## 3. THE SOFTWARE BASIS OF THE DACS

The DACS software consists of two realization levels:

1) the ER-DAS software suite;

2) high-level DACS software suite (of the radiometric facility level).

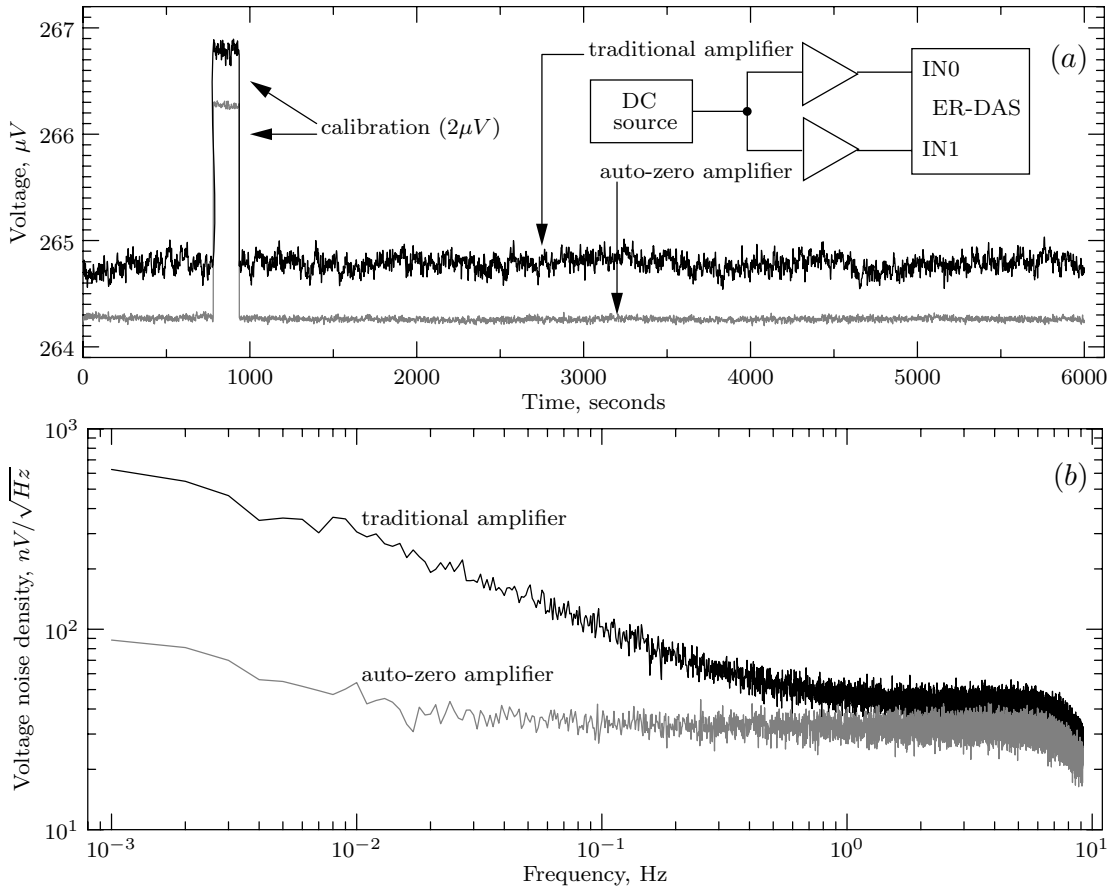


**Fig. 3.** Comparison of a DC amplifier based on traditional operational amplifiers (OpAmp) and of the preamplifier based on auto-zero OpAmps. (a)—Signals. The black curve shows the signal of a preamplifier based on a traditional OpAmp and the gray curve, the signal of a preamplifier with an auto-zero OpAmp. Also shown is the block diagram of the measurements. The signals were recorded simultaneously over 12 hours (the figure shows a less than two-hour long fragment of the records). (b)—The corresponding smoothed estimates of the spectral density of the amplitude. The estimates were made for full 12-hour records using a 50%-overlapping rectangular 1000-s-long window, followed by the smoothing of the spectra. The rise of the spectrum of the preamplifier with an auto-zero OpAmp (the gray curve) at low frequencies is due to $1/f^{\alpha}$-type fluctuations of the DC source (panel (a)).

### *3.1. ER-DAS Software Suite*

The ER-DAS software suite was developed for two microprocessors: the DSP processor and the communication processor.

DSP processor software.The DSP processor simultaneously reduces the data from four radiometers in real time. Figure 4 shows the sequence of the reduction stages for the data from a single radiometer. The algorithm of the processing of the radiometric signal (the algorithm of digital synchronous demodulation) has received its own name—Radiometric Digital Lock-in (RDL).

In the RDL algorithm the output signal of the modulation radiometer digitized in the analog subsystem (Fig. 4a) is transmitted to the input of the programmed switch operating at the modulation frequency. At this stage the phase of the modulated radiometer signal coincides with the phase of the modulating frequency so that the programmed switch synchronously separates the half-cycles of the modulated signals to two independent channels. As a result of operation at this stage two signals are produced (Fig. 4b). These signals are continuous in time, and the gaps in the signal that are due to switchings are filled with the average signal levels of the preceding half cycles. Thus each radiometric channel produces two digital data streams at the digitization frequency (32768 Hz), bringing the total number of such channels for a single ER-DAS system to eight.

The next two stages of digital processing are performed by two successively connected signal decimation units (Figs. 4c and 4d). Each of these software units reduces the sampling frequency of the data by a factor of 16, and as a result, the output signals from a single ER-DAS system have the form

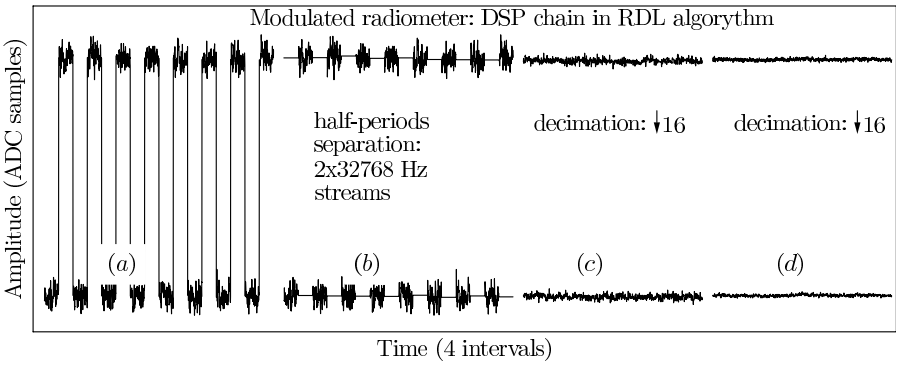


**Fig. 4.** RDL (Radiometric Digital Lock-in) algorithm in action.

of eight data streams with a sampling frequency of 128 Hz. As anti-aliasing filter the decimators use ICF (Integrator—Comb filter) single-stage digital filters, each of which has a cutoff frequency equal to 1/32 of the input signal bandwidth. The ICFs efficiently suppress three frequency components in the signal spectrum: the switching frequencies in auto-zero amplifiers (about 14 kHz), harmonics of the power-supply frequencies, and harmonics of the modulating signal frequency. The latter are suppressed most efficiently, because the modulation frequency and the frequencies at which decimators operate are exact multiples of the signal digitization frequency. Furthermore, breaking the radiometer signal into two streams reduces the contribution of modulation frequency harmonics in each of the new signals to the minimum possible level that is determined by the mean square deviation of radiometer noise.

Two-stage decimation is introduced because of the high gain of the ICFs (a $\times 16$ decimation results in a factor-of-32 gain in the algorithm employed) and limited digit capacity of integrator data words (32 bits). In the case of the use of the two's complement arithmetic the integrator data word length should be sufficient to accommodate the maximum difference between two successive counts (with the allowance for the ICF gain), see [8]. The total gain in the case of two-stage decimation should then be equal to $32 \times 32 = 1024$. In the case of the high level of input signals (e.g., radio interference) a programmed attenuator can be incorporated between the two decimation stages to ensure correct operation of the next stage.

Note that RDL algorithm does not complete the operation of synchronous demodulation of the signal. This operation is completed when the signals corresponding to two separate modulation half-cycles of a single radiometer are subtracted. This procedure can also be easily performed during the post reduction of observational data. As a result, we obtain extra information (compared to modulation radiometer) in the form of the signals of individual modulation half-cycles. These signals correspond to two total-power radiometers, each with a factor of $\sqrt{2}$ lower sensitivity compared to an ideal total-power radiometer. Thus the information that is completely lost in a traditional radiometer is totally preserved in this case.

The software for the communication processor includes:

1) the initial boot loader [7];

2) the embedded OS uClinux [7] with the support of TCP/IP, NTP time synchronization protocol, and the file system for SPI Flash (permanent memory at the Serial Peripheral Interface bus). This memory is used to store and modify all the application software for ER-DAS;

3) the original DSP processor—communication processor exchange driver;

4) the program for reading processed data from the DSP processor into the communication processor and for transmitting commands in the opposite direction via the exchange driver, and for the output of the result obtained into the computer network via TCP/IP protocol;

5) the program for loading the DSP processor from SPI Flash memory.

The entire software kit for the communication processor is loaded automatically when the voltage is supplied. It is also possible to remotely change in real-time mode both the software components and the operation mode of the entire system.

### *3.2. Software Kit for the DACS at the Radiometric Facility Level*

This software kit is built in accordance with the mulithreaded application technology and performs the following tasks:

1) integration of all radiometers (radiometric systems) into a single observational process;

2) control of radiometers and data acquisition in accordance with a unified observational/measurement program;

3) preliminary reduction of data in order to prepare their storage in the observational archive in the RATAN-FLEX format (RFLEX) [9]. This format is a version of the FITS data format adapted for the RATAN-600.

The software is written in C++ language for Linux OS and includes class and utility libraries for preparing observations and for data reduction. The object-oriented approach makes it possible to separate and formalize for the DACS such notions as the measurement facility (in the case of the RATAN-600 it is the secondary feed—reflector), item of equipment (radiometric system), data channel (one radiometer of a sensor), etc. C++ classes have been developed for all these notions (i.e., the necessary set of parameters and methods has been specified). The control parameters of the classes are stored in configuration files in the XML (eXtensible Markup Language) format. Such files describe both the measurement facility and the particular equipment set (radiometers/sensors). These descriptions determine the set of dynamically created classes and control flows. In other words, when the radiometric-facility level DACS starts, all lower-level hardware and software systems (e.g., ER-DAS) described in the configuration of the measurement system automatically join the measurement/observation process.

During its operation the DACS receives (with authorization and verification of permissions) user requests for setting/cancellation an observational program consisting of a description of a sequence of requested observations. The DACS performs observations in accordance with the schedule. Each completed observations is, after its automatic preliminary reduction, written in a RFLEX-format file and sent to the centralized data bank for archiving.

## 4. APPLICATION OF THE DACS+ER-DAS IN RADIO-ASTRONOMICAL OBSERVATIONS

Figure 5 illustrates an observation of 3C84 radio source using the radiometer of MARS-3 [10] facility in the 30 GHz domain (the microwave bandwidth $B = 5$ GHz). The signal pairs in Figs. 5a and 5b correspond to the individual modulation half-cycles of the beam-switching radiometer, the block diagram of which is shown in Fig. 5a. These are the output signals of the RDL algorithm (see above), where the data sampling frequency is reduced via decimation down to about 20 Hz in the post reduction of the data by the software of the radiometric-facility level DACS. A programmed eighth-order LPF with a Butterworth characteristic and zero phase characteristic developed by Tsybulev is used as the anti-aliasing filter before decimation. Figure 5b shows a fragment of the record shown in Fig. 5a, which corresponds to the radio-source related portion. Here the signal-to-noise ratio is further increased by applying an eighth-order digital LPF (also with a Butterworth characteristic and zero phase characteristic) with a cutoff frequency of 2.5 Hz. Note that the LPF employed is made as a filter with infinite impulse-response characteristic (IIR filter). Such a filter has a nonlinear phase characteristic, resulting in the distortion of the radio source and its shift along the time scale. Extra measures were undertaken to guarantee the zero phase characteristic of such a LPF result in zero group delay time in the filter preventing the distortion of the radio source and its shift along the time scale. This was achieved by double filtration via this IIR filter (but operating the in the fourth-order mode) and with the signal reversed in time before the second filtration as described, e.g., by Lyons [8].

Both small- and large-scale correlations between signals in individual modulation half-cycles can be seen in Fig. 5a. Small-scale correlations are mostly manifestations of the common radiometer microwave channel noise with a spectral density $1/f^{\alpha}$ (radiometer gain fluctuations). Large-scale correlations are the sum of the $1/f^{\alpha}$ type noise mentioned above and atmospheric radio emission fluctuations, which have the same form of power spectral density (PSD). The system temperature difference between the signals of two modulation half-cycles (about 1 K) is due to the difference between the losses in individual input channels at the radiometer entrance before the waveguide signal commutator (see the block diagram shown in Fig. 5a).

Figure 5c shows the result of the completion of synchronous demodulation of the signal of the modulation radiometer. This operation was performed in the process of post-reduction of data by subtracting the signals shown in Fig. 5b (the mean value of about 1 K that remained after the subtraction is

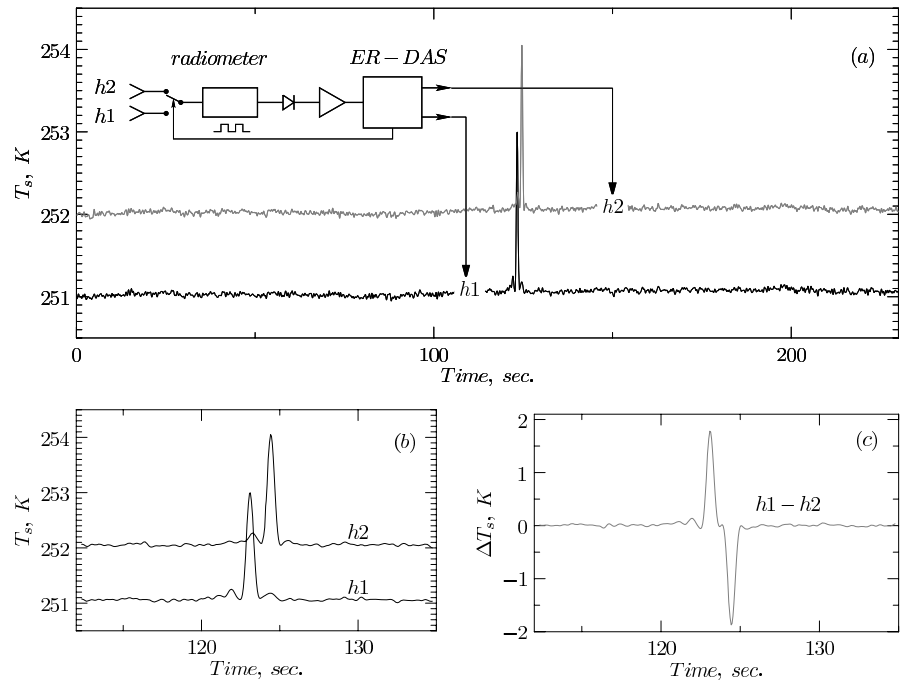


**Fig. 5.** Record of the transit of the 3C84 radio source across the fixed beam of the RATAN-600 at a frequency of 30 GHz (5-GHz wide microwave band). Panel (a)—the initial record of two individual modulation half-cycles corresponding to two spatially separated primary radiometer horns h1 and h2. Panel (b)—a fragment of record (a) with a radio source. Panel (c)—the result of subtracting the records of individual half-cycles: radiometer with software modulation.

also subtracted). We thus obtained the radiometer signal for the beam-switching radiometer. This signal is automatically cleaned of the $1/f^{\alpha}$ type noise due both to radiometer gain fluctuations and to the fluctuations of the atmospheric radio emission at the given wavelength. It goes without saying that the degree of the suppression of the noise types mentioned above is determined by the difference between the losses in the input channels of such a radiometer.

## 5. APPLICATION OF THE DACS+ER-DAS FOR MEASURING RADIOMETER GAIN FLUCTUATIONS

One of the important radiometer parameters is the amplitude of its gain fluctuations when the device operates in the total power radiometer mode. Refining the data on the gain fluctuations of modern radiometers may provide new information about the stability of the operation of these devices.

The computations and estimates are based on the following formula for the sensitivity of a total-power radiometer derived with the allowance for gain fluctuations (see, e.g., [11] or [12]):

$$\Delta T = T_s\sqrt{\frac{2\Delta F}{B} + \left(\frac{\delta G}{G}\right)^2}. \qquad (2)$$

Here $\Delta F$ is the low-frequency (LF) equivalent noise bandwidth (ENBW) of the radiometer determined by its low-pass filter (LPF); $B$, the width of the rectangular microwave band (microwave ENBW); $T_s$, the total equivalent noise temperature of the radio telescope+radiometer system; $\Delta T$, the r.m.s. deviation of noise temperature fluctuations recorded at the radiometer output; $G$ and $\delta G$, the radiometer gain and its variations, respectively. We can the write the following formula for relative noise fluctuations:

$$\left(\frac{\Delta T}{T_s}\right)^2 = \frac{2\Delta F}{B} + \left(\frac{\delta G}{G}\right)^2 = \left(\frac{\Delta T_w}{T_s}\right)^2 + \left(\frac{\delta G}{G}\right)^2, \qquad (3)$$

where we introduce the notation $2\Delta F/B = (\Delta T_w/T_s)^2$, and subscript $w$ indicates the white component of radiometer noise. Each term in (2) can be written in the form of integrals of the corresponding spectral power densities. We then have for the white component:

$$\left(\frac{\Delta T_w}{T_s}\right)^2 = \frac{2\Delta F}{B} = \frac{2}{B}\int_{F_1}^{F_2} df \qquad (4)$$

$$(\Delta F = F2 - F1).$$

The spectrum of radiometer gain fluctuations is known to have the form $A/f^{\alpha}$, e.g., [11]. In this paper we assume that parameters $\alpha$ and $A$ describe the relative spectral power density of radiometer gain fluctuations $(G(f)/G)^2$. We can then write the following formula:

$$\left(\frac{\delta G}{G}\right)^2 = A\int\limits_{F_1}^{F_2}\frac{1}{f^{\alpha}}df, \qquad (5)$$

and, in view of (3) and (4), we obtain:

$$\left(\frac{\Delta T}{T_s}\right)^2 = \int\limits_{F_1}^{F_2}\left(\frac{2}{B}+\frac{A}{f^{\alpha}}\right)df = \int\limits_{F_1}^{F_2}S(f)df, \qquad (6)$$

where we introduced the following notation

$$S(f) = \frac{2}{B}+\frac{A}{f^{\alpha}}. \qquad (7)$$

We further denote:

$$S_w = \frac{2}{B} = const, \qquad (8)$$

$$S_g(f) = \frac{A}{f^{\alpha}}. \qquad (9)$$

Here $S_w$ is the relative spectral power density of the white component of radiometer noise, which is computed from its known constant—the bandwidth $B$. Function $S_g(f)$ is the relative PSD of radiometer gain fluctuations, where parameters $A$ and $\alpha$ are to be estimated. Here $S(f)$ is the function of relative power spectral density of total fluctuations and it has the dimensions of [1/Hz]. Parameter $A$ in the formula for $S_g(f)$ has the same dimensions. It is evident that $A \equiv A/f^{\alpha}$ for $f = 1$ Hz ($\alpha > 0$).

It follows from Formula (6) that the measured estimate of the PSD of temperature fluctuations at the output of the total-power radiometer can be used to estimate the parameters $A$ and $\alpha$ of radiometer gain fluctuations (given $T_s$ and $B$). After determining these parameters we can integrate within the given limits both the total PSD estimate and its independent components (4) and (5).

The ER-DAS system can be used to measure gain fluctuations in the total-power radiometer mode without altering the radiometer design and without developing a special scheme for such measurements. The only thing to be done is to programmatically switch the RDL algorithm into the mode of continuous measurement of radiometer signal switching off the modulation signal at the same time. It is also necessary to perform sufficiently long measurements of the output signal of the total-power radiometer at constant (or at a sufficiently close to constant) $T_s$ to obtain a smoothed estimate of the PSD of the fluctuations of $T_s$. This estimate divided by $T_s^2$ can then be used for sufficiently accurate direct approximation by a function of the form (7).

Figure 6 shows successive stages of the practical process of the estimation of the parameters of function $S_g(f)$ (see formula 9):

1) Figure 6a demonstrates smoothed estimates of relative PSD of the fluctuations of $T_s$ (250 K and 500 K). The estimates are obtained by averaging individual spectra (Fast Fourier Transform (FFT), 100-second rectangular time window). We shifted the FFT window along the initial data with a 50% overlap (see [13] for a detailed description of the method). The total duration of laboratory observations under practically unchanged conditions for each $T_s$ was about 16 hours, and hence the total number of spectra averaged to obtain each smoothed PSD estimate is equal to 1152;

2) Figure 6b shows the relative PSDs obtained from the estimates shown in Fig.6a by dividing them by the squared known $T_s$ values. Thus the power spectrum of relative temperature fluctuations is independent of $T_s$ and contains the term $S_g(f)$ per se;

3) the result of the approximation of the estimated PSDs of relative fluctuations by the function of the form (7) in the frequency interval from 0.04 to 4 Hz is shown in Fig. 6c (parameters $\alpha, A$); The inferred parameters are used to reconstruct the desired spectrum $S_g(f)$ of radiometer gain fluctuations. The frequency band for approximation was chosen so that the spectrum in the selected frequency interval would indeed fit the two-component model described by formula (7).

Therefore, we obtain for the radiometer studied: $A = 1.6 \times 10^{-9} \pm 1.12 \times 10^{-11}(0.7\%)$, and $\alpha = 0.8 \pm 0.01$ (1.25%). This result is comparable to the results obtained in the NRAO for the 46-GHz radiometer based on the HEMT (High Electron Mobility Transistor), [14]: $A = 1.2 \times 10^{-8}$ and $\alpha = 0.9$. For comparison we can as well mention the parameters of one of the best radiometers of the early 1980s made at the RATAN-600, a noise adding radiometer (NAR) for the 8-cm wavelength, and a low-noise parametric amplifier at the input [15]: $A = 2.1 \times 10^{-10}$ and $\alpha = 1.25$.

The quoted errors of parameters $\alpha$ and $A$ include only the errors of the PSD approximation. Such small

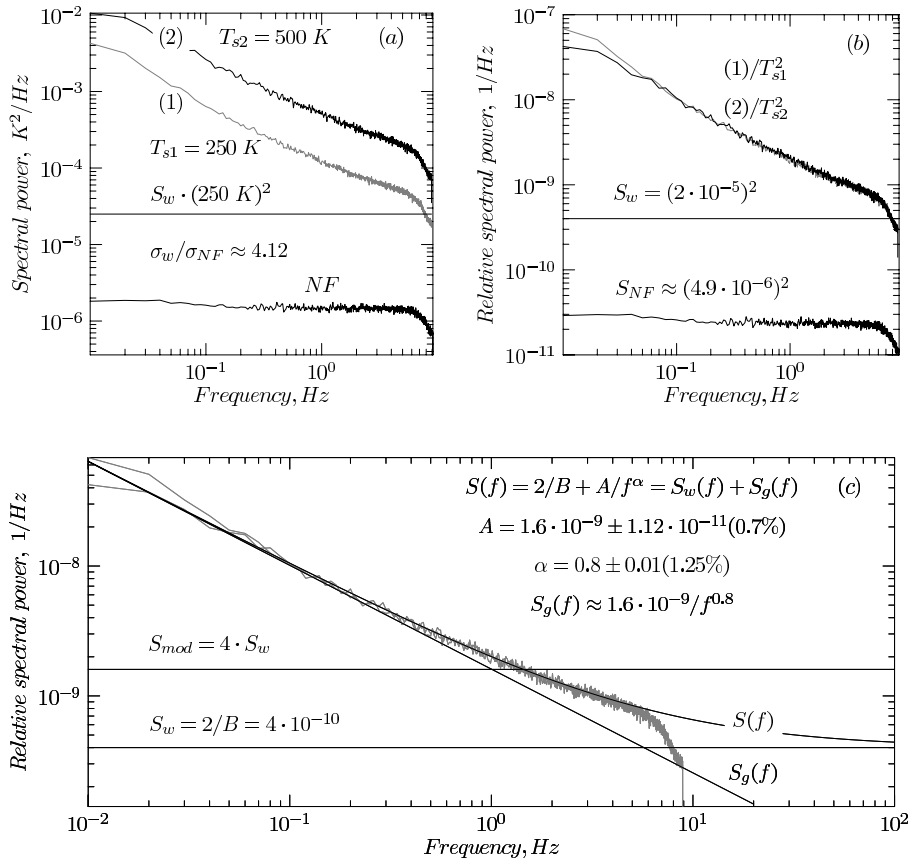


**Fig. 6.** Estimation of the gain fluctuations of the total-power radiometer of the MARS-3 radiometric system of the RATAN-600. The equivalent operating noise temperature of the radio telescope+radiometer system is $T_s = 250\ K$ and the microwave bandwidth, $B = 5$ GHz. Panel (a) The PSD estimates for the fluctuations of the effective noise temperature of the radiometer with $T_{s1} = 250$ K (curve (1)) and $T_{s2} = 500$ K (curve (2)). Here the $S_w \times (250\text{K})^2$ level corresponds to the spectral power density (PSD) of the ideal total-power radiometer with $T_s = 250$ K and a microwave bandwidth equal to $B$ (see above), $S_w = 2/B$. NF is the noise floor of the measurement system (preamplifier + ER-DAS). Panel (b) the relative PSDs of temperature fluctuations corresponding to the PSD estimates in panel (a) (their integration within the given limits yields $(\Delta T_s/T_s)^2$). Also show is the level $S_w$ of the relative fluctuations of the white component of the radiometer noise and the estimate $S_{NF}$ of the relative fluctuations of intrinsic noise. Panel (c) shows the approximation of the spectra shown in panel (b) by the function $S(f)$. After the estimation of parameters $\alpha$ and $A$ (their values are shown in the figure) the spectrum of radiometer gain fluctuations is computed (it is shown in the log-log scale—the curve $S_g(f)$). Here $S_{mod}$ is the level of the relative PSD for the corresponding modulation radiometer.

errors could be achieved by constructing a smoothed estimate for the PSD with a relative error of about 6%. The final error of parameter $\alpha$ must remain unchanged, because the slope of the spectrum was computed in a sufficiently wide frequency interval (three octaves). According to preliminary estimates, the resulting error for parameter $A$ should be increased by a factor of two to four.

Given the parameters of the relative PSD of detector gain fluctuations, we can estimate both $\delta G/G$, and the total noise at the radiometer output by integrating partially or completely the sum (7). It follows from

$$\int_{F_1}^{F_2} \frac{1}{f^\alpha} df = \begin{cases} \ln \dfrac{F2}{F1} & \alpha = 1 \\ \dfrac{F_2^{1-\alpha}}{1-\alpha} - \dfrac{F_1^{1-\alpha}}{1-\alpha} & \alpha \neq 1, \end{cases} \quad (10)$$

that at $\alpha = 0.8$ the integration of function $S(f)$ in the form (7) yields:

$$\int_{F_1}^{F_2} S(f) df = \frac{2}{B}(F_2 - F_1) + \frac{A}{0.2}(F_2^{0.2} - F_1^{0.2}). \quad (11)$$

Here the first term describes the white component of the radiometer noise and the second term, the gain

fluctuations. The contribution of both components depends on the choice of the integration limits and therefore the appropriate limits should be set for several estimate variants corresponding to real observing and measurement conditions.

The Table lists the results of computations for several characteristic LF bands. Here

$$\Delta T_w = T_s\sqrt{\frac{2(F2-F1)}{B}}, \qquad (12)$$

$$\Delta T_g = T_s\frac{\delta G}{G}, \qquad (13)$$

$$\Delta T = T_s\int_{F_1}^{F_2} S(f)df = \sqrt{\Delta T_w^2 + \Delta T_g^2}, \qquad (14)$$

where $\delta G/G$ is given by formula (5). Note that $\Delta T_g$ contributes substantially to the total estimate of $\Delta T$ fluctuations compared to the white component $\Delta T_w$ of the noise. The only exception is the variant of observation of the transit of point sources across the fixed beam of the radio telescope far from the polar region of the sky. In this case the total noise exceeds the white component by a factor of about two, which close to the sensitivity of the corresponding modulation radiometer.

It is evident from the Table that $\delta G/G$ does not exceed $10^{-4}$ for all the measurement variants listed despite the fact that the computations were made in the frequency intervals dominated by $A/f^\alpha$ noise. If we adopt $\delta G/G = 10^{-4}$ as a pessimistic estimate then $\delta G = 0.0001\,G$. This means that the gain fluctuations amount only to 0.01% of the total gain!

To better visualize the amplitude of fluctuations in the radiometer with the inferred parameters $\alpha$ and $A$, we can simulate sufficiently long realizations of $A/f^\alpha$ noise with different exponents $\alpha$. In this work we performed such a simulation using Matlab program powernoise.m developed as a part of speech recognition software [16]. We used this program to generate two different realizations of noise with the relative PSD of the form $A/f^\alpha$ (see Fig. 7) with the same amplitude $A = 1.6\times10^{-9}$ and two different exponents $\alpha$: $\alpha = 0.8$ ($S_{g,1}(f)$), and $\alpha = 1.6$ ($S_{g,2}(f)$). Exponent $\alpha = 1.6$ corresponds to a hypothetical radiometer of the 1970s. We also generated a realization of the low-frequency white noise with the relative PSD $S_w$, Fig. 7(a), for a radiometer with the microwave bandwidth of $B = 5\times10^9$ Hz (like the bandwidth of the MARS-3 facility mentioned above). We then successively added to this noise other noise components with spectra $S_{g,1}(f)$ and $S_{g,2}(f)$, and then multiplied the result by $T_s = 250$ K to obtain two realizations of simulated noise of two radiometers.

It is evident from the figure that the radiometer with gain fluctuations with a spectrum of $1/f^{0.8}$ (radiometer 1) demonstrates higher degree of long-term stability and lower noise level over the 11.5-day long experiment. On the contrary, the radiometer with $1/f^{1.6}$-type fluctuations (radiometer 2) demonstrates higher amplitude of small- and large-scale zero drift despite the fact that $T_s = 250$ K in both models.

## 6. CONCLUSIONS

As a result of the work performed, a new embedded data acquisition and control system for radiometers (ER-DAS) has been developed and its operation testing started at the RATAN-600 radio telescope. The extremely low intrinsic noise on the order of $(30\mathrm{nV}/\sqrt{\mathrm{Hz}})$ and the flat spectrum of the noise of the measurement system (long-term stability) allow radio-astronomical and radiometric measurements to be performed with very low absolute and relative errors. The long-term stability of the measurement system is of great importance for observations of point and, especially, extended objects in the total-power radiometer mode. Such observations can be made with radiometers with low spectral exponent of the $1/f^\alpha$ noise. ER-DAS can also be used as a precision DC amplifier plus ADC system to measure signals of physical parameter sensors in the frequency interval from zero to 8 kHz. The network service allows the ER-DAS system to be used as a part of distributed measurement facilities both on the RATAN-600 and other radio telescopes.

Software for the radiometric facility level data acquisition system has been developed and put into standard operation. This software kit has undergone successful testing over a one-year period within the framework of the Cosmological Gene project [17] as a part of one of the measuring facilities of the RATAN-600 ("type 2 feed", MARS-3 radiometric system) and proved to be highly reliable, flexible, and easy to operate.

Radio-astronomical observations using ER-DAS demonstrated that the use of RDL algorithm (see above) with delayed synchronous demodulation produce three signals from the output of a single modulation radiometer. Two signals correspond to individual modulation half-cycles and are the signals of a "quasi-radiometer" of total-power. The third signal can be obtained if necessary at the post-reduction stage—it is the signal from the output of the modulation radiometer. Such observational mode was earlier used on the RATAN-600 in the measurement facility of MARS-3 radiometric system, but the absolute

**Table.** Estimates of radiometer noise components for several variants of measurements. The rows 3, 4, and 5 correspond to the mode of the transit of objects studied across the fixed beam of the radio telescope in observations at large angular distances from the Celestial Pole

| $F1$ Hz | $F2$ Hz | $\Delta T_w/T_s$ $\times 10^{-5}$ | $\delta G/G$ $\times 10^{-5}$ | $\Delta T_w$ mK | $\Delta T_g$ mK | $\Delta T$ mK | $\Delta T/\Delta T_w$ | Remark |
|---|---|---|---|---|---|---|---|---|
| 0 | 1 | 2.00 | 8.94 | 5.0 | 22.4 | 22.9 | 4.58 | $\Delta F = F2 - F1 = 1Hz$ |
| 0 | 0.25 | 1.00 | 7.78 | 2.5 | 19.5 | 19.7 | 7.88 | $\Delta F = 1/4\tau, \tau = 1s$ |
| 0.2 | 2 | 2.76 | 6.44 | 6.89 | 16.1 | 17.5 | 2.33 | observation of point sources |
| 0.01 | 0.1 | 0.60 | 4.32 | 1.5 | 10.8 | 10.9 | 7.3 | extended objects |
| 0.003 | 0.03 | 0.33 | 3.83 | 0.82 | 9.51 | 9.54 | 11.6 | extended objects |

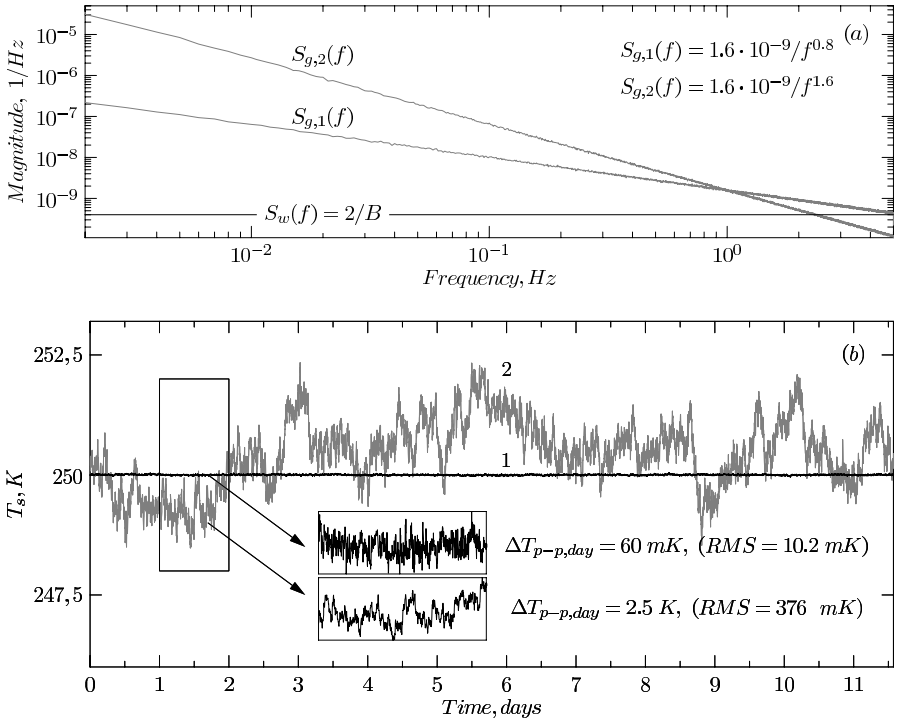


**Fig. 7.** Simulation of the behavior of two different radiometers 1 and 2 (corresponding to different spectra of gain fluctuations, $S_{g,1}(f)$ and $S_{g,2}(f)$), over 11.5 days. The parameters of the models are: $T_s = 250$ K and $B = 5$ GHz, two variants of $A/f^{\alpha}$ noise, where $\alpha = 0.8$ and $\alpha = 1.6$, $A = 1.6 \times 10^{-9}$. Panel (a) The relative PSDs. The horizontal line corresponds to the white component of radiometer noise. Panel (b) The signals corresponding to radiometers 1 and 2, in the temporal domain. Here $\Delta T_{p-p,day}$ are "peak-peak" fluctuations of the system temperature over one-day period. (See text for details). These fluctuations were computed in the frequency band $1.16 \times 10^{-5}$Hz $-$ 0.005Hz.

accuracy of measurements was poorer because of the zero drift in the measurement system. We thus expanded the range of possible modes of operation of the same radiometer and at the same time improved the measurement accuracy, which was one of the tasks to be addressed in the process of the development of the ER-DAS.

In the case of ER-DAS measurements one should pay attention to the absolute value of the radiometer signal. The radiometer calibrated in terms of equivalent noise temperature always shows the temperature of the radio-telescope + radiometer system ($T_s$) in measurements made using ER-DAS system, like, e.g., in Figs. 5a and 5b. This is achieved due to the use of precision DC amplifiers throughout the entire signal- measurement channel. The possibility of

measuring the true $T_s$ is one of the advantages of ER-DAS that makes it fundamentally different from other measurement systems based on traditional OpAmps. In the latter measurements of the same $T_s$ made at different time may yield different values because of the intrinsic zero drift of the measurement system.

We measured the fluctuations of the gain of one of the radiometers of MARS-3 facility (operating in the 30 GHz frequency range). Note that zero frequency (which corresponds to infinitely long observation of the radiometer signal) can be used as the lower integration limit in formula (5) for the PSD of gain fluctuations only if spectral exponent $\alpha < 1$, because otherwise the integral diverges. The first two rows in the Table correspond to the case of very long observation of the output signal of the radiometer with $1/f^{0.8}$ gain fluctuations, and $\delta G/G < 10^{-4}$. This result is appreciably better than the results obtained for radiometers of 1970s–1980s, when the stability levels of about $0.1\% - 1\%$/hour were achieved, like, e.g., in [11]. Furthermore, radiometers based on earlier-generation components had $\alpha$ parameters greater than unity. This allowed the radiometer stability to be estimated only over a limited time interval. The transition to new hardware components (HEMT transistors, Low-barrier Schottky diodes, precision integrated stabilizers) made it possible to improve the stability of modern radiometers. The very flat spectrum of the noise of the measurement system—Preamplifier + the ER-DAS system described here lends enough credibility that the radiometer gain fluctuations measured in this work are due to its microwave part with no contribution from the low-frequency measurement path.

A simulation of the signals of two radiometers with different gain fluctuations was performed (see Fig. 7). An analysis of two radiometer models shows that radiometer 2 (PSD $\sim 1/f^{1.6}$) needs to be regularly calibrated in the process of radio-astronomical observations. Such a calibration is performed using a dedicated calibrating noise source. The gain instability of radiometer 1 (PSD $\sim 1/f^{0.8}$) does not exceed 0.01%. Fixing the gain in such a radiometer allows its calibration to be performed much more rarely than in the previous case.

A technique of the measurement of radiometer gain fluctuations has been developed and used in practice. The need for such a methodological study is dictated by the rather free approach toward such measurements in radiometric practice, which sometimes leads to inconsistent and diverse results.

The measured parameters of $A/f^{\alpha}$ noise require more accurate identification of its source in the radiometer. I do not believe it to be self-evident to attribute this noise to gain fluctuations exclusively (this noise should rather be referred to as the fluctuations of the transmission coefficient of the entire radiometer). The noise factor variations of the low-noise amplifier also require further investigation. The relative contribution of the square-law detector to the total measured $A/f^{\alpha}$ noise is no entirely understood. All these problems are to be addressed in further studies.

## ACKNOWLEDGMENTS

This work was supported by the Russian Foundation for Basic Research (grants nos. 08-02-00486a, 08-02-05043-b, and 09-02-12169). I am grateful to all the staff members who took active part in the discussion of this work.

## REFERENCES

1. V.N. Cherenkov and P.G. Tsybulev, in *Abstracts of presentations at the 26th Radio-Astronomical Conference* (St.-Petersburg, 1995), p. 389.
2. A.B. Berlin and P.A. Friedman, in *Proceedings of the XXV URSI General Assembly, Lille, France*, Ed. by URSI (Gent, Belgium, 1996), p. 750.
3. P.A. Fridman, E.V. Bulaenko, and S.V. Tuzenko, in *Proceedings of the First International Conference and Exhibition, Digital Signal Processing and its Applications* (Moscow, Russia, 1998), III-E-55-66.
4. V.A. Stolyarov and P.G. Tsybulev, in *Abstracts of presentations at the 26th Radio-Astronomical Conference* (St.-Petersburg, 1997), p. 182.
5. P.G. Tsybulev, A.B. Berlin, N.A. Nizhel'skij, et al., Astrophysical Bulletin **62**, 193 (2007).
6. R.H. Dicke, Review of Scientific Instruments **17**, 268 (1946).
7. `http://docs.blackfin.uclinux.org`.
8. R.G. Lyons, *Understanding Digital Signal Processing*, 2nd ed. (Prentice Hall, NJ, USA, 2004).
9. O.V. Verkhodanov et al., *Report No. 233, Special Astrophysical Observatory of the Russian Academy of Sciences*, Nizhnii Arkhyz, 1994.
10. `http://www.sao.ru/hq/lrk/index.html.en`.
11. J. D. Kraus, *Radio Astronomy*, 2-nd ed. (Cygnus-Quasar Books, Powell, Ohio, 1986), p. 7-12.
12. N.A. Esepkina, D.V. Korol'kov, and Yu. N. Pariiskii, *Radioteleskopy i radiometry (Radio telescopes and radiometers)* (Nauka, Moscow, 1973), p. 319 [in Russian].
13. A.H. Nutall and G.C. Carter, Proc. IEEE **70**, 1115 (1982).
14. E.J. Wollack, Review of Scientific Instruments **66**, 4305 (1995).
15. V.Y. Golnev, D.V. Korolkov, and P.A. Fridman, Bull. Spec. Astrophys. Obs. **13**, 52 (1981).
16. M.A. Little et al., Biomed Eng Online **6**, 23 (2007) (`http://www.ncbi.nlm.nih.gov/pmc/articles/PMC1913514/`).
17. Yu. N. Parijskij, Astronomical and Astrophysical Transactions **19**, 265 (2000).